

Communication

Micromachining of Invar with 784 Beams Using 1.3 ps Laser Source at 515 nm

Petr Hauschwitz ^{1,2,*} , Bohumil Stoklasa ³, Jiří Kuchařík ³, Hana Turčičová ¹, Michael Písařík ¹, Jan Brajer ¹, Danijela Rostohar ¹, Tomáš Mocek ¹, Martin Duda ^{1,2} and Antonio Lucianetti ¹

¹ HiLASE Centre, Institute of Physics, Czech Academy of Sciences, Za Radnici 828, 25241 Dolní Brezany, Czech Republic; hana.turcicova@hilase.cz (H.T.); Michael.Pisarik@Hilase.cz (M.P.); jan.brajer@Hilase.cz (J.B.); danijela.rostohar@hilase.cz (D.R.); tomas.mocek@hilase.cz (T.M.); martin.duda@hilase.cz (M.D.); antonio.lucianetti@hilase.cz (A.L.)

² Faculty of Nuclear Sciences and Physical Engineering, Czech Technical University in Prague, Břehova 7, 115 19 Prague, Czech Republic

³ Meopta-optika, s.r.o., Kabelikova 1, 750 02 Prerov, Czech Republic; bohumil.stoklasa@meopta.com (B.S.); Jiri.Kucharik@meopta.com (J.K.)

* Correspondence: petr.hauschwitz@hilase.cz

Received: 17 June 2020; Accepted: 1 July 2020; Published: 2 July 2020



Abstract: To fulfil the requirements for high-resolution organic light-emitting diode (OLED) displays, precise and high-quality micrometer-scale patterns have to be fabricated inside metal shadow masks. Invar has been selected for this application due to its unique properties, especially a low coefficient of thermal expansion. In this study, a novel cost-efficient method of multi-beam micromachining of invar will be introduced. The combination of a Meopta beam splitting, focusing and monitoring module with a galvanometer scanner and HiLASE high-energy pulse laser system emitting ultrashort pulses at 515 nm allows drilling and cutting of invar foil with 784 beams at once with high precision and almost no thermal effects and heat-affected zone, thus significantly improving the throughput and efficiency.

Keywords: multi-beam micromachining; beam splitting; invar; shadow masks; OLED

1. Introduction

Invar is a Fe–Ni class alloy with unique properties such as excellent strength, impact toughness, processability and a low coefficient of thermal expansion [1]. Those properties are making invar very attractive for various industrial applications including bi-metal applications, storage tanks of liquefied natural gas, and shadow masks for production of organic light-emitting diodes (OLED) [2]. High-resolution shadow masks are crucial in red, green and blue evaporation process of organic luminous materials during the production of OLED displays [3]. The geometry, size and overall quality of holes in shadow mask are directly connected with OLED pixel quality [4]. Chemical etching is nowadays a common microfabrication method for production of OLED shadow mask [2]. However, it is a complicated multi-step process generally composed of coating, cleaning, exposure and an etching process with no control over the taper angle. Moreover, it is difficult to fabricate a pattern smaller than the material thickness due to isotropic manner of chemical etching and thus reach the high resolution required for future virtual reality displays [5,6].

As an alternative, laser micromachining provides high-quality, single-step and environmentally friendly approach without the use of chemicals. Laser microfabrication of shadow masks was investigated with several laser systems demonstrating 85 µm channels fabricated in polymethyl methacrylate with a CO₂ laser [7], 250 µm wide channels in wax using a CO₂ laser [8], 250 µm wide

lines in plastics and glass with the use of a Nd:YAG laser at the fundamental wavelength of 1064 nm [9], or 140 μm lines fabricated in a steel shadow mask using the third harmonics of a Nd:YAG laser [10]. However, to produce high-resolution shadow masks with small features in a range of a few tens of microns, ultrashort pulsed lasers have to be deployed [8,11–13]. Invar drilling with ultrashort laser systems was investigated, demonstrating 200 μm diameter in invar utilizing a 785 nm Ti:sapphire laser [4] and hole dimensions below 30 μm with excellent quality and minimal heat-affected zone [6].

However, the main drawback of ultrashort pulse laser micromachining is the processing speed which limits the widespread use in industry, especially in the case of a common single-beam direct laser writing approach. Moreover, with the emerging high-power ultrashort laser systems [14], high-quality invar micromachining becomes very inefficient as most of the laser power cannot be used. This is due to the necessity of processing close to the damage threshold to maintain high quality and minimal heat affected zone. Therefore, new techniques for rapid large-scale processing are required. The most promising rapid large-scale techniques include polygonal scanning systems [15,16], direct laser interference patterning [17,18] and multi-beam scanning approaches [19].

Beam splitting using a diffractive optical element (DOE) in a combination with galvanometer scanner and high-power ultrashort laser systems is a promising way to meet industry standards in high speed processing of large areas. DOE beam-splitter distributes the incident laser beam intensity into the desired far-field pattern which is usually an 1D or 2D array of beams. Each beam has the same characteristics as the original beam, except for pulse energy and angle of propagation [20]. Multibeam systems providing high throughputs due to beam splitting into 10–100 beamlets have recently become commercially available on the market able to drill holes in the range of 20 μm in diameter into 20 μm thick metal foils [21,22].

Consequently, this study aims to demonstrate a technology capable of producing microstructures in a cost-efficient way by introducing a prototype of a Meopta beam splitting, focusing and monitoring module. The module divides an initial high-quality beam into more than 700 beamlets for parallel processing of a thin invar foil. By utilizing the module in a combination with HiLASE high-energy pulse ultrashort laser system and a galvanometer scanner, it was possible to freely adjust the dimensions and geometry of produced microholes suitable for the production of OLED displays.

2. Materials and Methods

Invar (FeNi36) foils provided by Goodfellow GmbH (Friedberg, Germany) with a thickness of 20 μm and dimensions of 50 \times 50 mm were used as received ($R_a \sim 0.07 \mu\text{m}$). The foils were treated by Perla laser system from HiLASE (Dolni Brezany, Czech Republic), equipped with second harmonic generation module emitting at wavelength of 515 nm, with pulse duration of 1.3 ps, beam quality factor M2 better than 1.5, repetition rate of 1 kHz and pulse energy up to 10 mJ [14,23]. The generated beam (Figure 1c) was guided through the galvanometer scanner without F-theta lens into the optical module developed by Meopta-optika, s.r.o., consisting of a DOE beamsplitter, 100 mm focusing lens and a polarizing beamsplitter for pattern observation on the sample surface. The module is responsible for focusing and splitting the initial beam by means of diffractive optics into a matrix of 28 \times 28 beamlets with homogeneous distribution across the whole pattern and suppression of zero order diffraction. The module allows the separation distance between beamlets to be adjusted by changing the distance between the DOE and focusing lens. Beam splitter and camera allows to monitor the intensity, shape and focal position of each beamlet. The beamsplitter passes linearly polarized beam on to the sample surface. The reflected light from the sample with random polarization is then able to reach the camera. The separation distance between each beamlet on the sample plane was 150 μm . The sample was placed vertically on to the vacuum holder with an optional connection to the cooling water circuit. The whole setup is depicted in Figure 1.

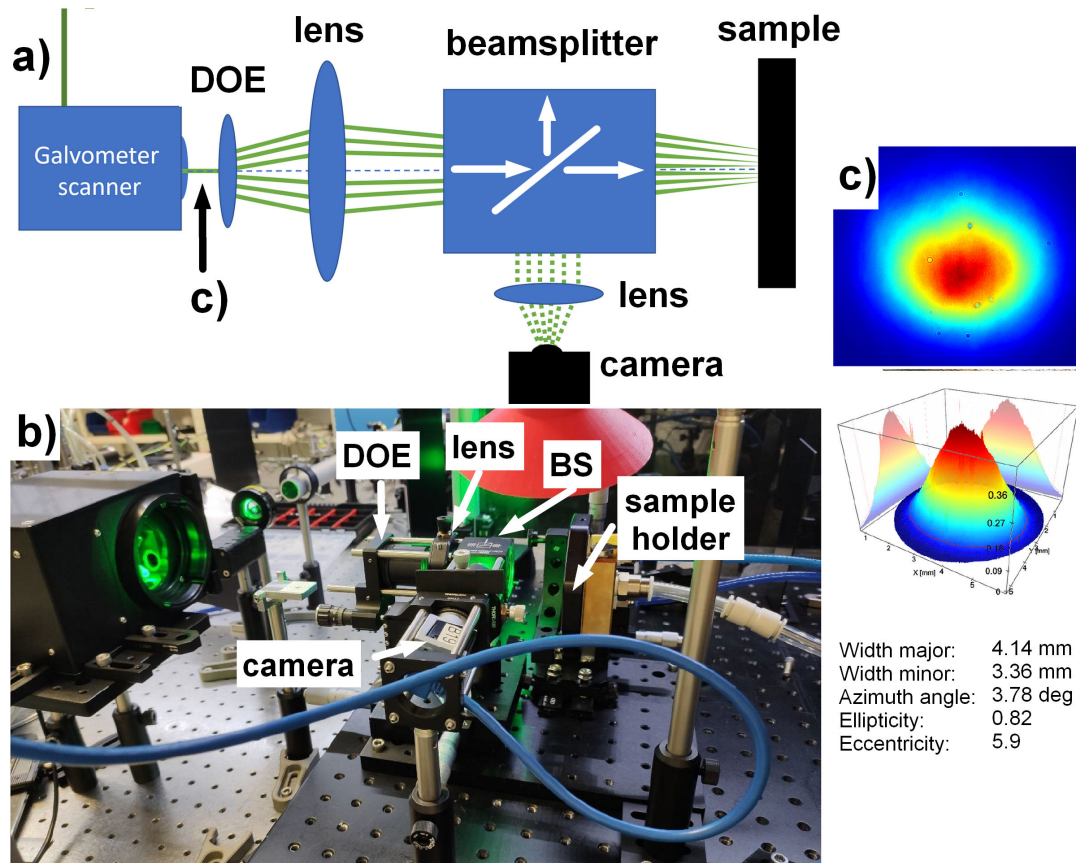


Figure 1. Schematics (a) and photo (b) of the experimental setup with a detail of input beam (c).

Topography of selected surfaces was analyzed with a laser scanning confocal microscope Olympus OLS 5000. The pattern shape and beamlets intensity distribution were captured by a Basler ace acA4024-29um camera with pixel size of $1.85 \mu\text{m}$.

3. Results and Discussion

The impact of the experimental setup misalignments on the resulting multi-spot pattern homogeneity, the tolerance of deviation angles during beam deflections affecting the pattern shape, as well as the laser and processing parameters for high-quality cutting and drilling have been studied in a set of experiments.

First, the pattern homogeneity had to be adjusted to reach the same intensity in each beamlet by tilting the beam-splitting element. The pattern shape was observed in real-time on a camera inside the Meopta beam-splitting module during the alignment, as depicted in Figure 2.

As shown in Figure 2, the pattern shape reflected from the sample surface exhibits undesired speckles, which can be further improved by mirror polishing of the sample. In addition to pattern homogeneity, the working plane was easily found by observing the pattern on camera as the sharp beam profile of each beamlet (inset of Figure 2b) can be observed only when the sample is located exactly in the focal plane.

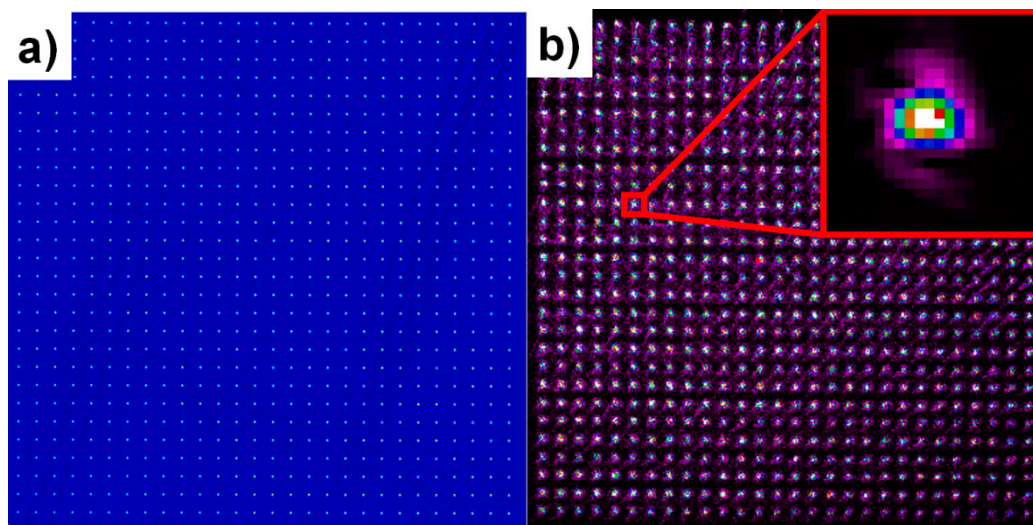


Figure 2. Final pattern shape on camera in a sample plane (a) and the same pattern reflected from the sample surface (b).

In the next step, the sample was irradiated with 100,000 consecutive laser pulses with energy of 0.6 mJ which corresponds to the fluence of 0.28 J/cm^2 for each beamlet. The first experiments revealed extensive heat accumulation connected with a large heat-affected zone and interconnection of microholes into one hole in the center of the pattern due to extensive heating and melting (Figure 3a). Consequently, the samples were placed on a water-cooled holder to minimize the effect of heat accumulation, as depicted in Figure 3b.

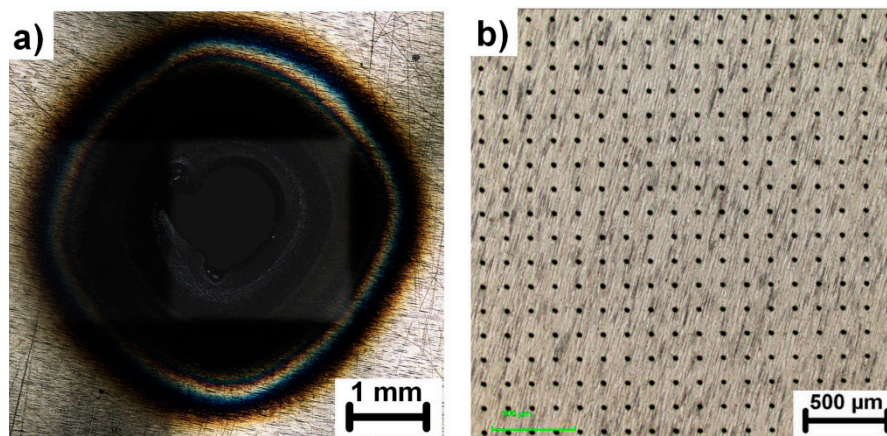


Figure 3. Overview of the heat affected zone on the sample processed without water-cooled holder (a) compared to the sample processed with the water-cooled holder (b). Both samples were processed with the same fluence of 0.28 J/cm^2 and 100,000 pulses.

To determine an optimal processing window for high-quality multi-beam drilling, different combinations of laser parameters were analyzed. First, the ablation threshold for the simultaneous drilling of 784 holes was estimated. Figure 4a presents a microhole ablated close to the ablation threshold with 100,000 pulses and pulse energy of 0.3 mJ in the initial beam (beamlet fluence of 0.15 J/cm^2). No ablation was observed for pulse energies below 0.3 mJ, hence it is considered as the ablation threshold.

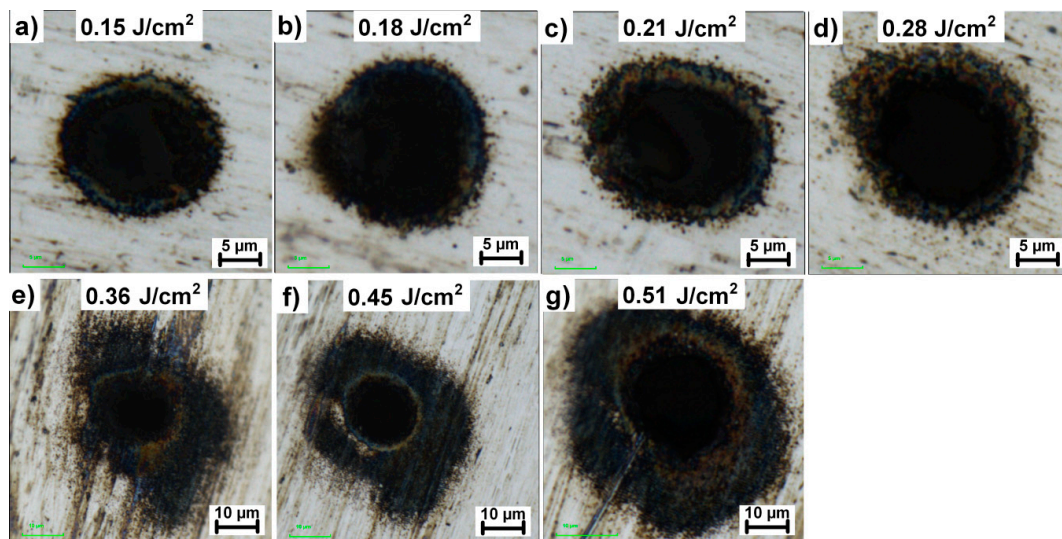


Figure 4. Evolution of microhole quality and heat affected zone with the increase in fluence. Sample is irradiated with 100,000 consecutive laser pulses. (a–d) gentle ablation regime, (e–g) high fluence regime.

The extension of the heat-affected zone and overall hole quality have been examined using different pulse energies in the range of 0.3 mJ to 1.2 mJ which correspond to the beamlet fluence of 0.15 J/cm² to 0.51 J/cm², as shown in Figure 4.

In line with the results presented in Figure 4, two ablation regimes have been identified. The highest quality microholes have been reached in a gentle ablation regime for fluences up to two-times the ablation threshold, i.e., up to 0.28 J/cm². In this case, the extension of the heat-affected zone was found to be less than 3 µm. By increasing the fluence over this value, the quality of microholes significantly deteriorated due to the extensive heat-affected zone. Moreover, as shown in Figure 5a, the removal rate (ablated volume per time and power) for microholes drilled in a higher fluence regime over 0.28 J/cm² is much smaller compared to lower fluences.

This phenomenon may be explained by the decrease in beam quality connected with high pulse energies which may overcome the tolerances of a diffractive beamsplitter and thus affect the intensity distribution within the beamlet. This issue will be further addressed in the following research.

On the other hand, the removal rate is sharply increasing with the fluence in the gentle ablation regime reaching the peak around 0.28 J/cm², which was identified as the optimal fluence for effective drilling.

Furthermore, the number of pulses required for piercing the sample have been determined (Figure 5b). With the threshold fluence of 0.15 J/cm² at least 2.5 million pulses were required to pierce through the 20 µm thick invar foil, thus removing less than 0.01 nm per pulse. By increasing the fluence above the ablation threshold, the sample was pierced with less than 700,000 pulses for fluences between 0.18 J/cm² and 0.28 J/cm². The lowest number of pulses required for piercing the foil was in the case of 0.28 J/cm² with only 500,000 pulses, which is in accordance with the optimal removal rate value. For the higher fluence regime, the sample was pierced only in the case of 0.36 J/cm² after exposition with 1 million pulses. Higher fluences did not lead to cutting through the invar foil even after 3 million pulses. Therefore, the optimal processing window for effective micromachining of invar foil has been identified as 0.18 J/cm² to 0.28 J/cm².

Additionally, the effect of laser parameters on the microhole diameter input/output aspect ratio have been studied. As demonstrated in Figure 5c, the aspect ratio decreases with higher fluences as well as with increasing number of pulses. Similarly, the shape of the exit diameter also improves with a higher number of applied pulses (Figure 6).

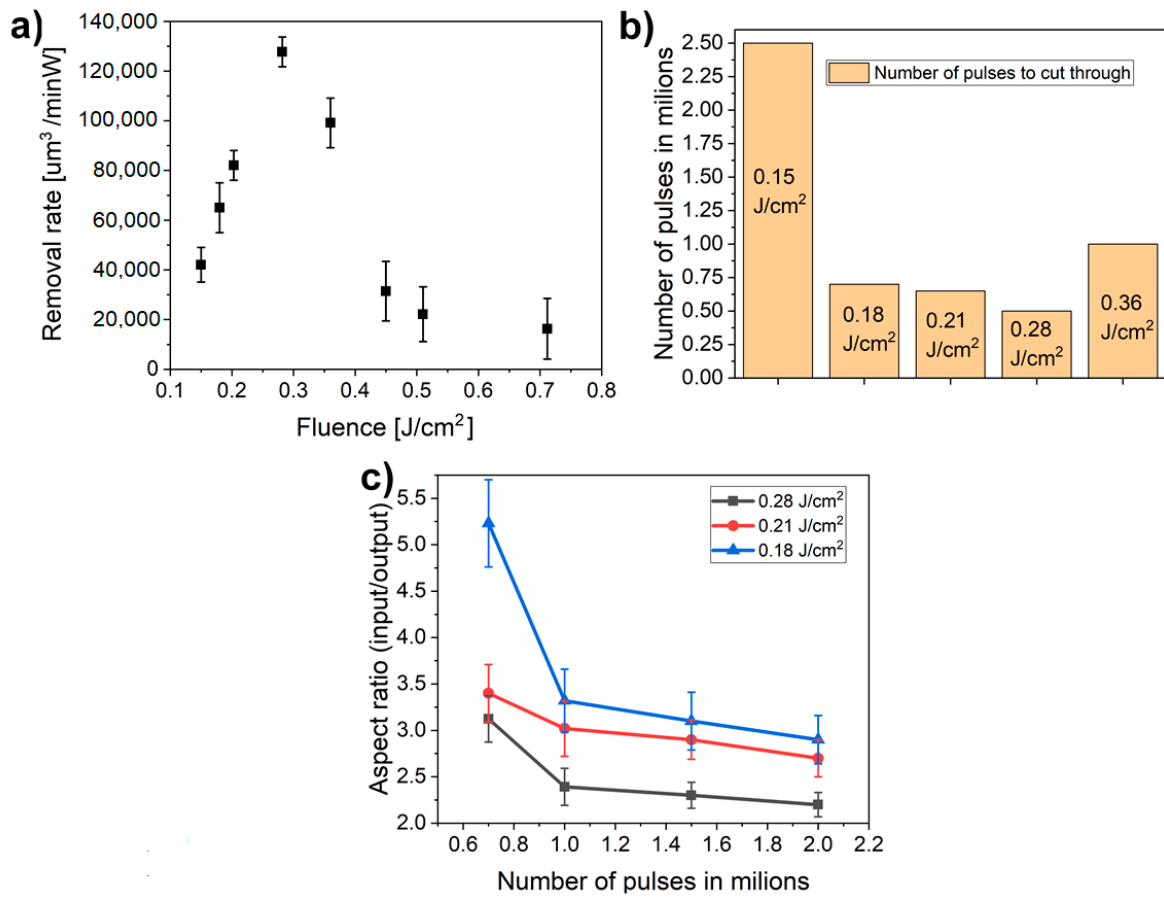


Figure 5. (a) Removal rate as a function of fluence; (b) Number of pulses necessary to cut through the whole sample; (c) Evolution of the aspect ratio as a function of number of pulses.

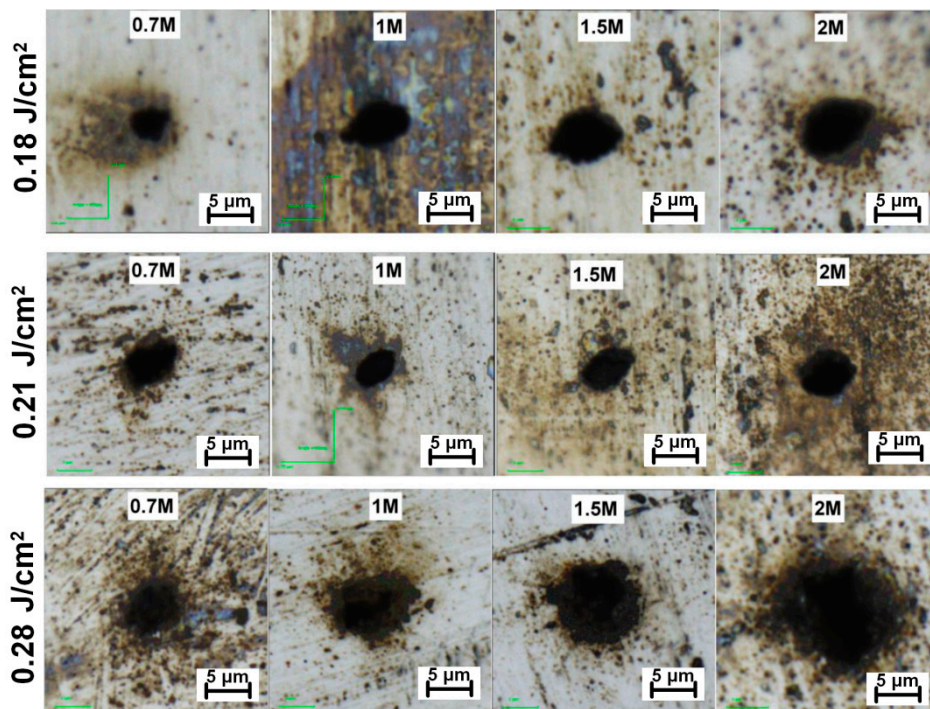


Figure 6. Geometry evolution of exit hole diameters with increasing number of pulses from 0.7 million to 2 million pulses.

Generally, the exit microhole diameter is larger and less elliptical for higher fluences and pulse counts, as demonstrated in Figure 6. The best aspect ratio and circularity were reached for the sample irradiated with 2 million pulses and 0.28 J/cm^2 per beamlet.

Following up on the optimal parameters, a galvanometer scanner was deployed to deflect the beam in a small area between microholes to fabricate different geometries on the invar foil. Since the separation distance between produced microholes is $150 \mu\text{m}$, the square with a side width of $100 \mu\text{m}$ was chosen for the cutting experiment. To improve cutting efficiency, the input cut width was increased by cutting 15 squares with the same center position and decreasing diameter per $3 \mu\text{m}$ for each square. The cutting speed was adjusted to 1 mm/s to ensure high enough overlapping of $\sim 95\%$ with the laser repetition rate of 1 kHz . The cutting results are depicted in Figure 7.

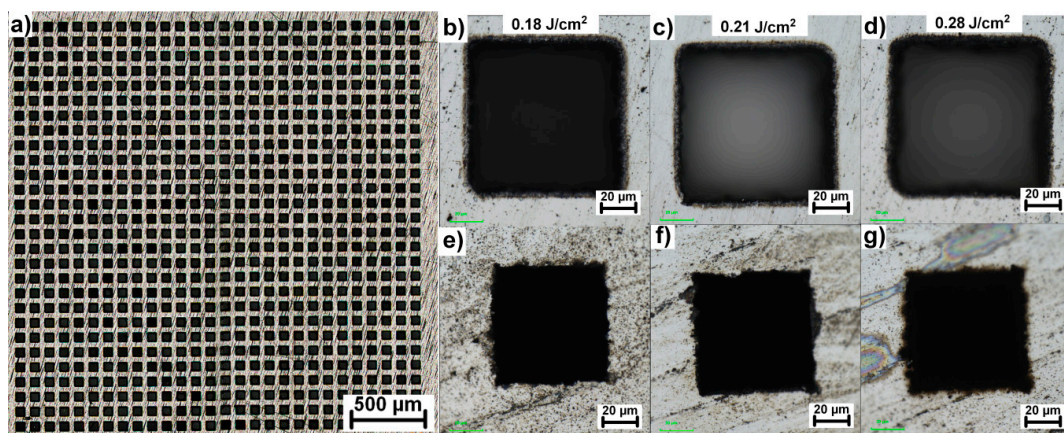


Figure 7. (a) Overview of a pattern cut with a combination of 28×28 beamsplitter and galvanometer scanner; (b–d) details of a square cuts fabricated with different fluences inside the optimal processing window and 400 overscans and their corresponding exit sides (e–g).

As demonstrated in Figure 7, it was possible to fabricate square geometries and cut through the invar foil with all 784 beams at once. The complete penetration was reached for 700, 440 and 250 overscans for the fluences of 0.18 J/cm^2 , 0.21 J/cm^2 , and 0.28 J/cm^2 , respectively. In addition, the consistency of square shape and their separation distance was measured on 20 randomly selected squares across the pattern confirming the exact same parameters across the pattern with the standard deviation smaller than $3 \mu\text{m}$ in all cases.

4. Conclusions

Utilization of a Meopta beam-splitting, focusing and monitoring module in a combination with HiLASE high-energy pulse laser system emitting ultrashort pulses at 515 nm resulted in efficient cutting and drilling of invar foil simultaneously by 784 beamlets, arranged in a matrix of 28×28 beamlets. The features of optical module allow the setup to be aligned quickly to reach homogeneous intensity distribution across the whole pattern, as well as focus adjustment. By determining the ablation threshold, optimal fluence levels and pulse counts, the optimal processing window for effective high-quality drilling and cutting with heat affected zone below $3 \mu\text{m}$ has been identified as 0.18 J/cm^2 to 0.28 J/cm^2 . The combination of galvanometer scanning head and beam-splitting module enabled multi-beam fabrication of square-shaped microholes with adjustable dimensions. With the use of this solution, the throughput can be increased 7 times compared to the state of the art commercial multi-beam systems and more than 700 times compared to the single beam approach, thus showing high potential for significant improvement in the fabrication speed and efficiency during the production of invar shadow masks.

Author Contributions: Conceptualization, B.S., M.P.; Methodology, B.S., M.P., P.H.; Validation, B.S., M.P., P.H., J.B.; Formal analysis, B.S., J.K.; Investigation, P.H., B.S., H.T., J.K.; Resources, B.S., H.T., M.D.; Writing-Original

Draft, P.H.; Writing, Review and Editing, P.H., J.K., D.R., A.L., M.D.; Visualization, P.H.; Supervision, B.S., J.B., M.P., T.M.; Project administration, J.B., B.S.; Funding acquisition, B.S., M.P., J.B., T.M. All authors have read and agreed to the published version of the manuscript.

Funding: This work is a result of project TN01000008 NCK CEPO—New methods for laser micromachining. This work was co-financed by the European Regional Development Fund and the state budget of the Czech Republic (project HiLASE CoE: Grant No. CZ.02.1.01/0.0/0.0/15_006/0000674) and from the European Union's Horizon 2020 research and innovation programme (Grant agreement NO 739573) and by the Ministry of Education, Youth and Sports of the Czech Republic (Programme NPU I Project No. LO1602).

Conflicts of Interest: The authors declare no conflict of interest. The funders had no role in the design of the study; in the collection, analyses, or interpretation of data; in the writing of the manuscript, or in the decision to publish the results.

References

1. Ono, F.; Hamatani, Y.; Mukumoto, Y.; Komatsu, S.; Ishikawa, N.; Chimi, Y.; Iwase, A.; Kambara, T.; Mueller, C.; Neumann, R. Modification of Fe–Ni Invar alloys by high-energy ion beams. *Nucl. Instrum. Methods Phys. Res. Sect. B Beam Interac. Mater. At.* **2003**, *206*, 295–298. [[CrossRef](#)]
2. Kim, C. Production of shadow-mask-improved technology. *J. Mater. Process. Technol.* **2002**, *127*, 409–418. [[CrossRef](#)]
3. Shin, H.Y.; Suh, M.C. A study on full color organic light emitting diodes with blue common layer under the patterned emission layer. *Org. Electron.* **2014**, *15*, 2932–2941. [[CrossRef](#)]
4. Chung, I.-Y.; Kim, J.-D.; Kang, K.-H. Ablation drilling of invar alloy using ultrashort pulsed laser. *Int. J. Precis. Eng. Manuf.* **2009**, *10*, 11–16. [[CrossRef](#)]
5. Kim, S.H.; Choi, S.G.; Choi, W.K.; Yang, B.Y.; Lee, E.S. Pulse electrochemical machining on Invar alloy: Optical microscopic/SEM and non-contact 3D measurement study of surface analyses. *Appl. Surf. Sci.* **2014**, *314*, 822–831. [[CrossRef](#)]
6. Choi, W.; Kim, H.Y.; Jeon, J.W.; Chang, W.S.; Cho, S.H. Vibration-assisted femtosecond Laser drilling with controllable taper angles for AMOLED fine metal mask fabrication. *Materials* **2017**, *10*, 212. [[CrossRef](#)]
7. Klank, H.; Kutter, J.P.; Geschke, O. CO₂-laser micromachining and back-end processing for rapid production of PMMA-based microfluidic systems. *Lab Chip* **2002**, *2*, 242–246. [[CrossRef](#)]
8. Fan, Y.; Li, H.; Yi, Y.; Foulds, I.G. Laser micromachined wax-covered plastic paper as both sputter deposition shadow masks and deep-ultraviolet patterning masks for polymethylmethacrylate-based microfluidic systems. *J. Micro/Nanolithogr. MEMS MOEMS* **2013**, *12*, 049701. [[CrossRef](#)]
9. Tahir, B.A.; Ahmed, R.; Ashiq, M.G.; Ahmed, A.; Saeed, M.A. Cutting of nonmetallic materials using Nd: YAG laser beam. *Chin. Phys. B* **2012**, *21*, 044201. [[CrossRef](#)]
10. Shiu, P.; Knopf, G.; Ostojic, M.; Nikumb, S. Rapid fabrication of tooling for microfluidic devices via laser micromachining and hot embossing. *J. Micromech. Microeng.* **2008**, *18*, 025012. [[CrossRef](#)]
11. Rizvi, N.H.; Apte, P. Developments in laser micro-machining techniques. *J. Mater. Process. Technol.* **2002**, *127*, 206–210. [[CrossRef](#)]
12. Kumar, A.; Gupta, A.; Kant, R.; Akhtar, S.N.; Tiwari, N.; Ramkumar, J.; Bhattacharya, S. Optimization of laser machining process for the preparation of photomasks, and its application to microsystems fabrication. *J. Micro/Nanolithogr. MEMS MOEMS* **2013**, *12*, 041203. [[CrossRef](#)]
13. Heo, J.; Min, H.; Lee, M. Laser micromachining of permalloy for fine metal mask. *Int. J. Precis. Eng. Manuf. Green Technol.* **2015**, *2*, 225–230. [[CrossRef](#)]
14. Smrž, M.; Novák, O.; Mužík, J.; Turčičová, H.; Chyla, M.; Nagisetty, S.S.; Vyvlečka, M.; Roškot, L.; Miura, T.; Černohorská, J.; et al. Advances in high-power, ultrashort pulse DPSSL technologies at HiLASE. *Appl. Sci.* **2017**, *7*, 1016. [[CrossRef](#)]
15. Mincuzzi, G.; Gemini, L.; Faucon, M.; Kling, R. Extending ultra-short pulse laser texturing over large area. *Appl. Surf. Sci.* **2016**, *386*, 65–71. [[CrossRef](#)]
16. De Loor, R. Polygon scanner system for ultra short pulsed laser micro-machining applications. *Phys. Proced.* **2013**, *41*, 544–551. [[CrossRef](#)]
17. Voisiat, B.; Gedvilas, M.; Indrišiūnas, S.; Račiukaitis, G. Picosecond-laser 4-beam-interference ablation as a flexible tool for thin film microstructuring. *Phys. Proced.* **2011**, *12*, 116–124. [[CrossRef](#)]

18. Hauschwitz, P.; Jagdheesh, R.; Alamri, S.; Rostohar, D.; Kunze, T.; Brajer, J.; Kopeček, J.; Mocek, T. Fabrication of functional superhydrophobic surfaces on carbon fibre reinforced plastics by IR and UV direct laser interference patterning. *Appl. Surf. Sci.* **2019**, *508*, 144817. [[CrossRef](#)]
19. Gillner, A.; Finger, J.; Gretzki, P.; Niessen, M.; Bartels, T.; Reininghaus, M. High power laser processing with ultrafast and multi-parallel beams. *J. Laser Micro Nanoeng.* **2019**, *14*, 129–137.
20. Katz, S.; Kaplan, N.; Grossinger, I. Using Diffractive Optical Elements: DOEs for beam shaping—fundamentals and applications. *Opt. Photonik* **2018**, *13*, 83–86. [[CrossRef](#)]
21. Holtkamp, J.; Eifel, S.; Ryll, J. Material Processing with Ultrashort-pulsed Lasers: Potentials—Requirements—Approaches. *Laser Tech. J.* **2014**, *11*, 36–39. [[CrossRef](#)]
22. Holtkamp, J. Pulsar Photonics: Innovative Beam Forming Concepts, Swissphotonics. Available online: <https://swissphotonics.net/libraries.files/holtkamp> (accessed on 1 July 2020).
23. Duda, M.; Novák, O.; Chyla, M.; Smrž, M.; Mocek, T. Balancing the conversion efficiency and beam quality of second harmonic generation of a two-picosecond Yb: YAG thin-disk laser. *Laser Phys.* **2020**, *30*, 025405. [[CrossRef](#)]



© 2020 by the authors. Licensee MDPI, Basel, Switzerland. This article is an open access article distributed under the terms and conditions of the Creative Commons Attribution (CC BY) license (<http://creativecommons.org/licenses/by/4.0/>).